Ground displacements revealed by A-DInSAR analysis in the Germano iron mining complex before and after the Fundão Dam collapse using Sentinel-1 data

José C. Mura,[a,*] Fabio F. Gama,[a] Waldir R. Paradella,[a] Cleber G. de Oliveira,[b] and Thiago G. Rodrigues[b]
[a]National Institute for Space Research, São José dos Campos, Brazil
[b]VISIONA Tecnologia Espacial, São José dos Campos, Brazil

Abstract. Advanced differential SAR interferometry (A-DInSAR) has been used as an effective monitoring tool in mining environments. This work presents an investigation of surface displacement in the Germano iron mining complex (Mariana, Minas Gerais, Brazil), where on November 5, 2015, the Fundão tailings dam collapsed. Initially, the analysis was performed with 14 Sentinel-1 images, acquired from May 8, 2015, to November 4, 2015, and focused on the Fundão dam before its rupture to detect prior signs of surface deformations. The analysis after the Fundão dam collapse was conducted in the Germano area using 43 Sentinel-1 images, acquired from November 16, 2015 to May 15, 2017, and aimed at detecting surface displacement on the remaining infrastructure, the Sela&Tulipa and Selinha dikes and the main Germano tailings dam, which were directly or indirectly affected by the accident. The results reveal precursor signals of surface displacement at the Fundão dam prior to rupture, particularly on the left abutment setback sector where the collapse started according to a witness, reaching accumulated values of up to −60 mm. The results provided by the A-DInSAR analysis after the dam collapse indicate a stability in the Sela&Tulipa and Selinha dikes as well as in the main Germano dam, which is corroborated by *in situ* topographic measurements. On the auxiliary dikes within the Germano reservoir, accumulated displacement of up to −90 mm caused by settlements and continuous traffic of vehicles was detected. In addition, the detected accumulate displacement within the reservoir showed values of up to −120 mm, in general caused by settlements of the waste dry material due to the inactivity of the mining process. The investigation emphasized the important role that satellite-based A-DInSAR can play in mitigating possible accidents and for operational planning and risk assessment in mining operations. © *2021 Society of Photo-Optical Instrumentation Engineers (SPIE)* [DOI: 10.1117/1.JRS.15.034513]

Keywords: Mariana; Fundão; tailing dam; collapse; advanced differential SAR interferometry; Sentinel-1.

Paper 210236 received Apr. 20, 2021; accepted for publication Jul. 22, 2021; published online Aug. 13, 2021.

1 Introduction

The Germano iron mining complex is located in the municipality of Mariana, Minas Gerais; it accounted for 72.5% of the Brazilian iron reserves (19.4 billion of tons) and 68.8% of national production in 2013.[1] This complex includes open pit mines, waste piles, industrial plants, pipelines, and a system of dams and dikes (Germano's main dam, Fundão dam, Santarém dam, Sela&Tulipa dike, and Selinha dike). The Fundão dam was a large structure with dimensions of about 500-m length and main walls of 110-m in height. The Fundão reservoir stored about 55 million cubic meters of tailings materials in November 2015. On November 5, 2015, the Fundão dam collapsed, spilling about 32.6 million of cubic meters of mining waste from the dam (60% of its capacity at the time). The dam collapse produced mud waves that destroyed buildings and infrastructure in the rural districts of Bento Rodrigues, Paracatu de Baixo, and Gesteira, with 19 dead victims, and contaminated 668 km of watercourses from the Doce

*Address all correspondence to José C. Mura, jose.mura@inpe.br

1931-3195/2021/$28.00 © 2021 SPIE

Downloaded From: https://www.spiedigitallibrary.org/journals/Journal-of-Applied-Remote-Sensing on 31 Aug 2021
Terms of Use: https://www.spiedigitallibrary.org/terms-of-use

River basin to the Atlantic Ocean, with environmental damage in the Brazilian Atlantic Forest, estuarine, coastal, and marine areas.[2] The released tailings flowed over to the supporting structures of the Sela&Tulipa and Selinha dikes on the side walls of the main Germano dam and concomitantly hit over the Santarem dam, causing partial erosion to its main structure.

According to the technical final report of the Fundão disaster, the dam collapse was related to liquefaction of solid materials, i.e., when the sandy tailings lose their mechanical resistance and present fluid behavior.[3] Another aspect to be considered for the failure was the series of small seismic shocks that occurred earlier. Three events were detected around 90 min prior to the dam collapse, with regional Richter magnitudes (mR) between 1.4 and 2.6. A small event was detected around the time of the accident, and four more events occurred over the following days with magnitudes ranging from 1.3 to 1.9 mR.[4] Despite these movements having been small, it is likely that they accelerated the failure process that was well in progress.[3]

A-DInSAR techniques based on multi-temporal satellite SAR acquisitions have improved the ability to detect temporal changes in deformation phenomena. These techniques are represented by two main classes: the small baseline subset (SBAS) technique,[5] which relies on a stack of multi-referenced differential interferograms and is sensitive to stable and distributed scatterers, and the persistent scatterer interferometry (PSI) technique,[6–8] which is based on a stack of master-referenced differential interferograms and identifies pixels with scattering properties that do not vary much with time (persistent scatterers). These techniques have been used to measure ground displacement in underground mines[9–17] and in open pit mines and related infrastructures.[11,18–27] A-DInSAR techniques provide the ability to monitor mining areas with large synoptic coverage, without the need to install equipment and field campaigns, providing reliable measurements of ground displacement and point-to-point accuracy at the millimeter scale with a dense sample grid. Geodetic (total station/prisms, leveling, and GPS) and non-geodetic methods (piezometers, inclinometers, and ground-based radar) have been applied for monitoring mining areas. The reliability and accuracy of these methods are undeniable; nevertheless, they can provide measurements only for specific points or sectors of the area where the instrumentation has been placed; in addition, the monitoring can be time consuming and requires fieldwork. However, they are indispensable when it comes to real-time monitoring, so a good strategy is to use both techniques to get the information of a specific sector (ground-based instruments) and a synoptic coverage with space born SAR data.

The investigation presented in this work was divided in two monitoring periods. The first analysis was performed with 14 available Sentinel-1 images, acquired from May 8, 2015, to November 4, 2015, and focused on the Fundão dam before its rupture to detect prior evidences of ground deformations. The second analysis was conducted after the Fundão dam collapse in Germano mining complex area, using 43 Sentinel-1 images, acquired from November 16, 2015, to May 15, 2017, and aimed at detecting surface displacement on the remaining infrastructure, the Sela&Tulipa and Selinha dikes and the main Germano tailings dam, which were directly or indirectly affected by the accident. The results of both monitoring periods were compared with available *in situ* monitoring data, based on geodetic surveying using on total station and mini reflective prisms.

2 Study Area

The bedrocks of the site of the Germano iron mining complex consist of ironstones known as itabirites from the Paleoproterozoic age (2.1 to 2 Ga) and are associated with a platformal sequence of the Minas Supergroup, where massive and soft iron ores were formed due to the supergene process acting during the Neogene over products associated with hydrothermal enrichments.[1] This mining complex is an important iron producer in Brazil, which is explored by the Brazilian SAMARCO Mineração S.A., with open pit mines, waste piles, industrial plant, pipelines, tailings, and water dams. The Germano tailings dam is the biggest of the Germano complex, with an estimated capacity of 116 million of cubic meters, whereas the Fundão tailing dam had about 55 million cubic meters of tailings materials in November 2015.[1]

According to the final expert report (immediate causes of the failure of the Fundão dam),[3] the following chronological and remarkable events took place before the dam failure. In 1976, the

Downloaded From: https://www.spiedigitallibrary.org/journals/Journal-of-Applied-Remote-Sensing on 31 Aug 2021
Terms of Use: https://www.spiedigitallibrary.org/terms-of-use

main Germano dam was built according to the upstream method; it was designed to store different types of tailings. During construction, the sand was first deposited to form a pile that retained the sludge discharged separately behind it; the sands, in turn, were retained by a rockfill starter dam at the downstream toe of the stack. In 1977, the operation started with the implantation of a 70-m high start dike, and a crest at the elevation of 849.5 m. Over time, the Germano dam crest rose progressively upstream over previously deposited tailings, until reaching an elevation of 899 m. From the beginning, until 1995, the Germano reservoir only received sandy waste, but from 1977, slime materials were also deposited, mainly in the central, north, and northwest sectors of the reservoir, and by 2005, the existing tailings facilities at the Germano dam were nearing capacity. A new tailings site was chosen in the adjacent Fundão Valley, with the initial layout purpose of physically separating sands and slimes, with sands deposited behind dike 1 and slimes behind dike 2 in the Fundão reservoir. Slime retention requires that the sands deposited between the two dikes always remain at a higher elevation throughout the raising process. The two dikes were strategically positioned for sands and slimes in 70% and 30% proportion of the total received from all plants. Dike 2 was originally planned to deposit sands behind a compacted earthfill Starter Dam (Fundão dam), and then raise it by the upstream method to increase progressively its capacity. These sands, in turn, would retain slimes deposited behind them such that the two materials would not intermingle. To preserve the free draining characteristics of the sands, a 200-m beach width was required to prevent water-born slimes from settling near the dam crest, where they would impede drainage. An efficient drainage system at the base of the Starter Dam would allow water to drain from the sands, reducing saturation. However, the first incident occurred in 2009 shortly after the Starter Dam was completed due to defects in the base drain. A revised design moved a new drainage blanket at a higher elevation and changed the design concept so that more widespread saturation was allowed and accepted. This increase in the extent of saturation introduced the potential for sand liquefaction. Incidents associated with slimes and water management occurred over an extended period of time in 2011 and 2012 while the new design was being constructed. The 200-m beach width criterion was often not met during operation, with water invading up to 60 m from the crest. This allowed slimes to settle in areas where they were not supposed to exist. In late 2012, another incident occurred when a large concrete conduit beneath the Fundão dam's left abutment was found to be structurally deficient and unable to support further loading. Due to this, the dam could not be raised over it until it had been abandoned and filled with concrete. To keep the mining operations in the interim, the alignment of the Fundão dam at the left abutment was set back from its former position. This condition placed the embankment directly over the previously deposited slimes, which gathered all of the conditions necessary for triggering the liquefaction. As the dam raising continued, surface seepage began to appear on the left abutment during 2013, causing the growing of saturated mass of tailings sands. By August 2014, the replacement blanket drain intended to control this saturation reached its maximum capacity. Meanwhile, the slimes beneath the embankment were responding to the increasing load being placed on them by the rising embankment, which ultimately caused the sands liquefaction. As the softer slimes were loaded, they compressed and simultaneously deformed laterally, squeezing out in a process known as lateral extrusion. The immediate upper sands were forced to conform to this movement, causing a reduction in the horizontal tension that confined them. This allowed the sands to, in effect, be pulled apart and in the process become looser. A related aspect of the failure was the series of three small seismic shocks that occurred about 90 min earlier. At that time, the left abutment of the dam had reached a precarious state of stability. Although the movements were quite small and the associated uncertainties large, this additional movement is likely to have accelerated the failure process that was already well advanced. The liquefaction flowsliding was the consequence of a chain of events and conditions that led to the rupture of the Fundão dam. A change in original design (setback) brought about an increase in saturation that introduced the potential for liquefaction. As a result, slimes existed beneath the embankment and were subjected to the loading its raising imposed, consequently initiating a mechanism of extrusion of the slimes and pulling apart of the sands as the embankment height increased.

After the accident, structural reinforcement works were carried out in the Sela&Tulipa and Selinha dikes and on the main Germano dam foot. SAMARCO Company has deployed different kind of *in situ* stability monitoring, such as total station/prisms and ground-based radar. Figure 1

Downloaded From: https://www.spiedigitallibrary.org/journals/Journal-of-Applied-Remote-Sensing on 31 Aug 2021
Terms of Use: https://www.spiedigitallibrary.org/terms-of-use

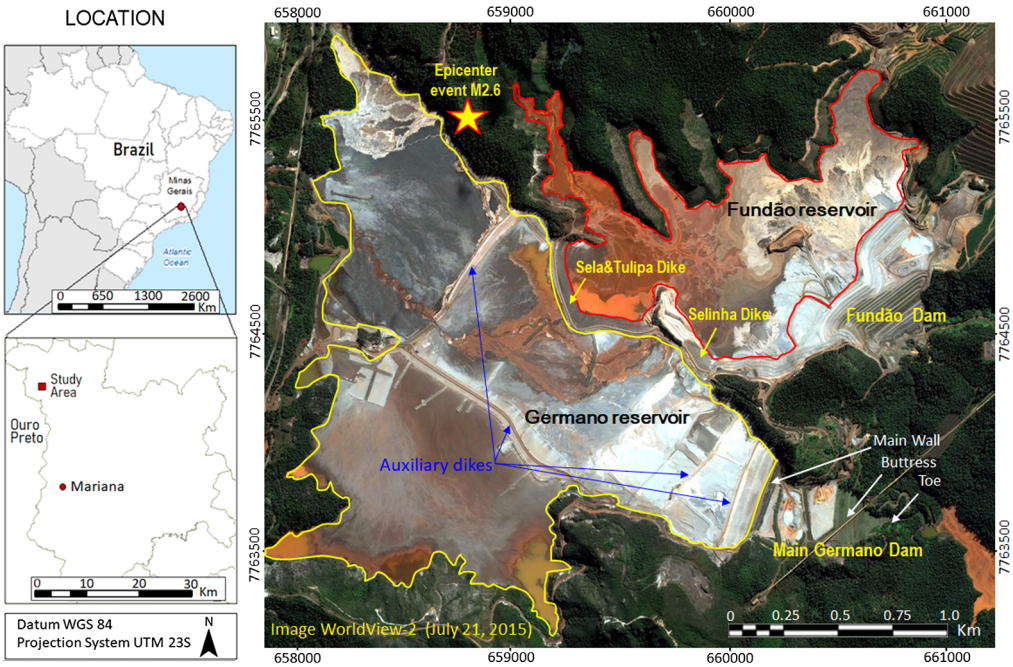

Fig. 1 Study area of the main structures at the Germano iron mining complex.

shows the location of the Fundão dam before the accident analyzed first and the remaining structures of the Germano mining complex (Sela&Tulipa dyke, Selinha dike, and the main Germano dam) analyzed after the accident in this study.

3 Data Set

The first analysis before the accident was carried out with 14 available SLC images from Sentinel-1A, IW mode, VV polarization, descending orbits, 41.19-deg incidence angle, 12-day revisit, from March 08, 2015, to November 04, 2015 (Table 1). The orbit files were updated using the European orbital data from the European Space Agency repository of Sentinel-1 auxiliary files [Precise Orbit Ephemerides files (POEORB)] for all S1 scenes to calculate the interferograms more accurately.

The analysis of the ground displacement after the collapse of the Fundão dam was carried out in the entire study area, using 43 SLC images from Sentinel-1A and B, IW mode, VV polarization descending orbits, 41.19-deg incidence angle, from November 16, 2015, to May 15, 2017 (Table 2).

Table 1 Acquisitions date of the Sentinel-1A images before the accident.

Acquisition date of S1 images			
1	May 8, 2015	8	August 12, 2015
2	June 1, 2015	9	August 24, 2015
3	June 13, 2015	10	September 17, 2015
4	June 25, 2015	11	September 19, 2015
5	July 7, 2015	12	October 11, 2015
6	July 19, 2015	13	October 23, 2015
7	July 31, 2015	14	November 4, 2015

Downloaded From: https://www.spiedigitallibrary.org/journals/Journal-of-Applied-Remote-Sensing on 31 Aug 2021
Terms of Use: https://www.spiedigitallibrary.org/terms-of-use

Table 2 Date acquisitions of the Sentinel-1A and B data after the accident.

Acquisition date of S1 images							
1	November 16, 2015	12	April 20, 2016	23	September 11, 2016	34	January 15, 2017
2	November 28, 2015	13	May 2, 2016	24	September 23, 2016	35	January 27, 2017
3	December 22, 2015	14	May 14, 2016	25	September 29, 2016	36	February 8, 2017
4	January 3, 2016	15	May 26, 2016	26	October 11, 2016	37	February 20, 2017
5	January 15, 2016	16	June 7, 2016	27	October 23, 2016	38	March 4, 2017
6	January 27, 2016	17	July 1, 2016	28	November 4, 2016	39	March 16, 2017
7	February 8, 2016	18	July 13, 2016	29	November 16, 2016	40	March 28, 2017
8	February 20, 2016	19	July 25, 2016	30	November 28, 2016	41	April 9, 2017
9	March 3, 2016	20	August 6, 2016	31	December 10, 2016	42	May 3, 2017
10	March 27, 2016	21	August 18, 2016	32	December 22, 2016	43	May 15, 2017
11	April 8, 2016	22	August 30, 2016	33	January 3, 2017		

A digital elevation model (DEM), with 1 m of spatial resolution, was generated from WordView-2 stereo images with a spatial resolution of 0.5 m, acquired on July 27, 2015, for the analysis before the Fundão dam collapse. For the analysis after the dam collapse, a DEM, with 1 m of spatial resolution, was generated from a Pléiades 1-A tri-stereo images with a spatial resolution of 0.5 m, acquired on June 19, 2016. In both cases, they were generated using the rational polynomial coefficients (RPC) model, available on the PCI Geomatica OrthoEngine software, that makes full use of the auxiliary parameters of the WordView-2 and Pléiades 1-A tri-stereo images.

4 Methodological Approach

Continuous Earth observation by SAR satellites has improved the capability for detecting temporal changes of deformation phenomena. A time series of SAR images acquired on the same area allows for the generation of the differential interferograms, providing the detection of the temporal ground displacement in the line-of-sight (LOS) direction. An interferogram derived from two images acquired within a time span Δt has a phase contribution from topography, ground displacement, atmosphere, baseline error, and noise. The topographic phase can be removed using a known DEM, with the phase related to the topographic error remaining; thus the observed interferometric phase of a measured point (MP) is represented as[6]

$$\phi_{Ob\_\Delta t} = \phi_{dr} + \phi_{\varepsilon h} + \phi_{atm} + \phi_{\beta} + \phi_{\eta}, \tag{1}$$

where ϕ_{dr} is the phase due to the displacement in the LOS direction, $\phi_{\varepsilon h}$ is the topographic phase error, ϕ_{atm} is the atmospheric phase delay, ϕ_{β} is the residual phase due to orbit errors, and ϕ_{η} is the random phase noise.

To detect precursory signals of the ground displacement in the Fundão dam before its rupture and the monitoring of the remaining dam and dikes after the accident using the Sentinel-1 data, we used an integration of two A-DInSAR techniques aiming to improve the detection of ground displacement in a large coverage area in full resolution. The combined techniques aim to explore the different characteristics of the scatterers within the resolution cell; while PSI extracts the phase change by analyzing stable and dominant scatterers, the SBAS technique is also sensitive to stable but distributed scatterers.[28] The processing flow of the proposed methodology to make the PSI analysis more effective[22,24] is shown in Fig. 2.

Downloaded From: https://www.spiedigitallibrary.org/journals/Journal-of-Applied-Remote-Sensing on 31 Aug 2021
Terms of Use: https://www.spiedigitallibrary.org/terms-of-use

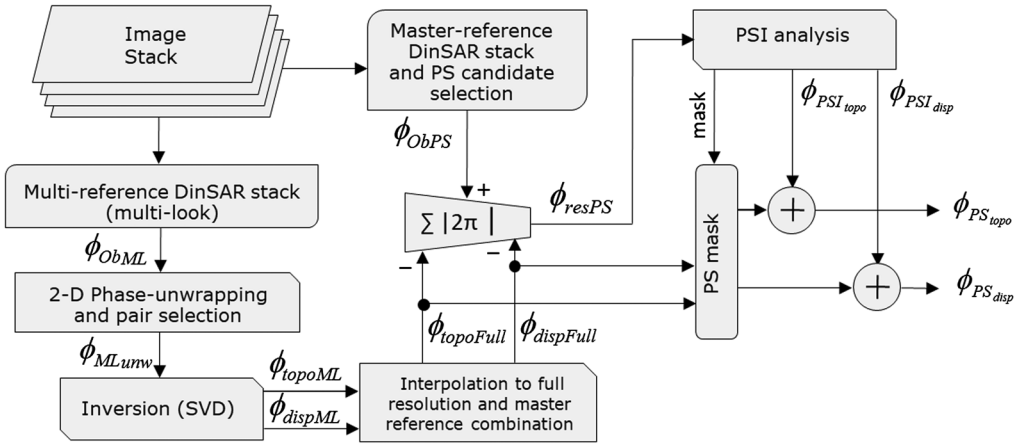

Fig. 2 Processing flow of the methodological approach.

According to the processing flow, first a multi-reference stack of interferograms is generated and spatially filtered using a multi-look technique (ϕ_{ObML}); these interferograms are unwrapped (ϕ_{MLunw}) with the minimum cost flow (MCF) algorithm[29] and then used to estimate initially the topographic phase error (ϕ_{topoML}) and the ground displacement phase (ϕ_{dispML}), based on the singular value decomposition (SVD) inversion method,[30] as used in the SBAS processing.[5] These results are then interpolated to full resolution and rearranged in relation to the master image (ϕ_{topoFull}, ϕ_{dispFull}). The second step is the generation of a master-referenced stack of interferograms and the selection of the PS candidates (ϕ_{ObPS}). Then, the phase of each PS is subtracted modulo 2π with the topographic phase error and displacement phases from the SBAS analysis, at the same coordinate as the PS. The resulting residual phase (ϕ_{resPS}) then goes through the PSI analysis. Finally, the results of the PSI (ϕ_{PSItopo}, ϕ_{PSIdisp}) are added to the results of the SBAS for only the PS position (PS_{mask}) that passed the PSI analysis criteria, resulting in a final estimation of the topographic phase error (ϕ_{PStopo}) and ground displacement phase (ϕ_{PSdisp}) for the MPs.

5 Data Processing

5.1 *Period Before the Collapse*

The data collection in this period occurred from March 8, 2015, to November 4, 2015. After the image co-registration, a multi-referenced stack was generated using the normal baseline restriction of up to 150 m and the time interval between interferometric pairs of up to 40 days, providing a total of 29 interferograms [Fig. 3(a)]. They were spatially filtered using a multi-look technique of 5×1 (five in range) pixels, and then they were unwrapped using the MCF algorithm.[29] After the visual inspection, four interferograms were removed from the stack due to the critical unwrapping errors. From the stack of selected unwrapped interferograms, the topographic errors and the ground displacement were estimated based on the SVD inversion method. The master referenced stack of interferometric pairs, based on 14 deramped SLC images, was built in relation to the image acquired on July 31, 2015, considering the low perpendicular baseline dispersion and its position nearly at the center of the time series to maximize the interferometric coherence, as shown in Fig. 3(b).

The estimation of PS candidates was based on the amplitude dispersion index (Ferretti et al.[7]) and low spectral diversity at each pixel position of the stack of the co-registered images in full resolution. A reference point was selected in a stable area, and its phase value was subtracted (modulo-2π) from all PS phase values, creating a set of differential interferograms for each PS. The stack of interferograms for PSI analysis is related to the master image, and the phase related to the ground displacement and topographic phase errors, previously found with a multi-referenced stack, were spatially interpolated to full resolution and then reorganized according

Downloaded From: https://www.spiedigitallibrary.org/journals/Journal-of-Applied-Remote-Sensing on 31 Aug 2021
Terms of Use: https://www.spiedigitallibrary.org/terms-of-use

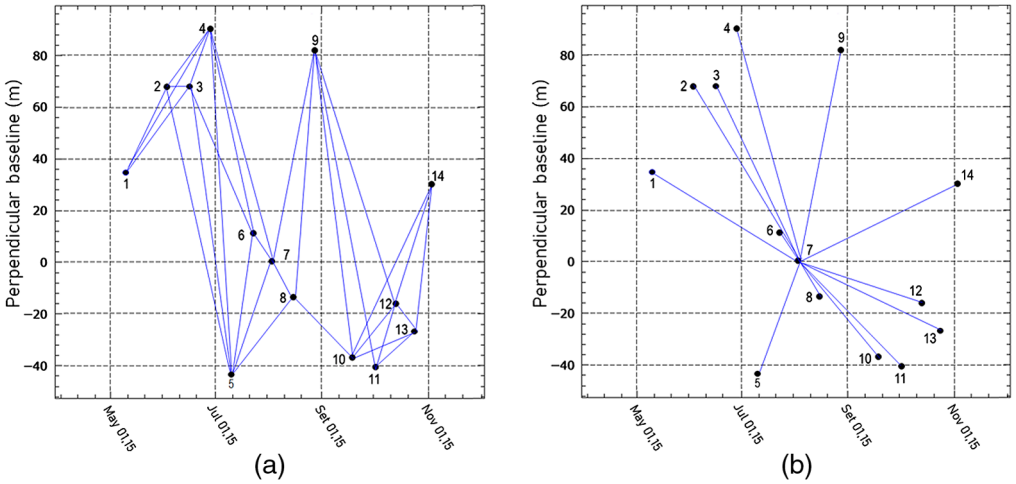

Fig. 3 (a) Multi-referenced and (b) master referenced pairs from 14 S1A images before the accident.

to the single reference. Finally, they were subtracted in modulus 2π from the PS phase, resulting in a residual phase that was subjected to PSI analysis, as shown in Fig. 2.

PSI analysis was performed using the interferometric point target analysis approach[7] implemented in GAMMA RS software,[31] where the topographic residual error estimation was based on the linear dependence with the values of perpendicular baseline, and the residual ground displacement was estimated through a linear regression between time and phase variation for each PS. The phase standard deviation for the linear regression error was limited to 1.35 radians, allowing for rejection of PS out of this error limit. This limit was empirically chosen to remove noisy PS while preserving the PS density.

The atmosphere-induced phase accounts for most of the linear regression deviation (residues) related to the deformation. The residue layers were spatially filtered (200×200 samples) and subtracted from the stack to remove the interference from the atmospheric phase. The remaining phase components account for the residual linear and nonlinear deformation phase and topographic phase error. After a step-wise iteration, the final results of the PSI analysis were added to the multi-referenced analysis results, previously described, with only the PS that fulfilled the processing constraint being added; this resulted in the final estimation of the ground displacement and topographic error.

5.2 *Period After the Collapse*

The data collection in this period occurred from November 16, 2016, to May 15, 2017, totaling 43 images. The multi-referenced A-DInSAR stack was generated using the normal baseline restriction of up to 150 m and the time interval between interferometric pairs of up to 25 days, providing a total of 75 interferograms [Fig. 4(a)]. They were spatially filtered using a multi-look technique of 5×1 (5 in range) pixels unwrapped using the MCF algorithm. After the inspection, nine interferograms were removed from the stack due to the critical unwrapping errors. Topographic errors and the ground displacement were estimated based on the SVD inversion method from the stack of selected interferograms. The master referenced stack of interferometric pairs was built in relation to the image acquired on August 06, 2016, shown in Fig. 4(b). The PSI processing occurred in the same way as performed in the first period.

6 Results and Discussion

The ground displacement detected in the Fundão dam and surrounding area, from March 8, 2015, to November 4, 2015, presents a more pronounced pattern of displacement rate at the center crest and on the left setback sector of the dam, as shown in Fig. 5(a). The displacement

Downloaded From: https://www.spiedigitallibrary.org/journals/Journal-of-Applied-Remote-Sensing on 31 Aug 2021
Terms of Use: https://www.spiedigitallibrary.org/terms-of-use

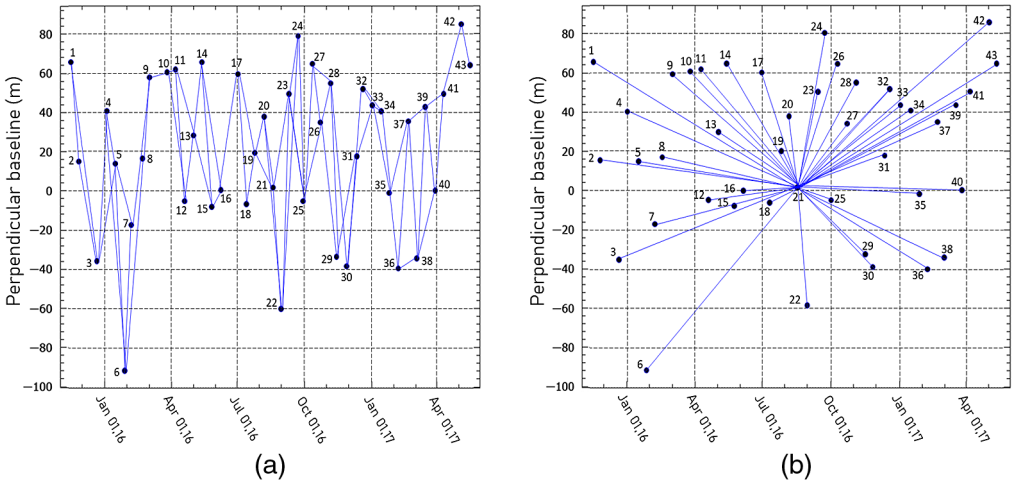

Fig. 4 (a) Multi-referenced and (b) master-referenced pairs from 43 S1A, B images after the accident.

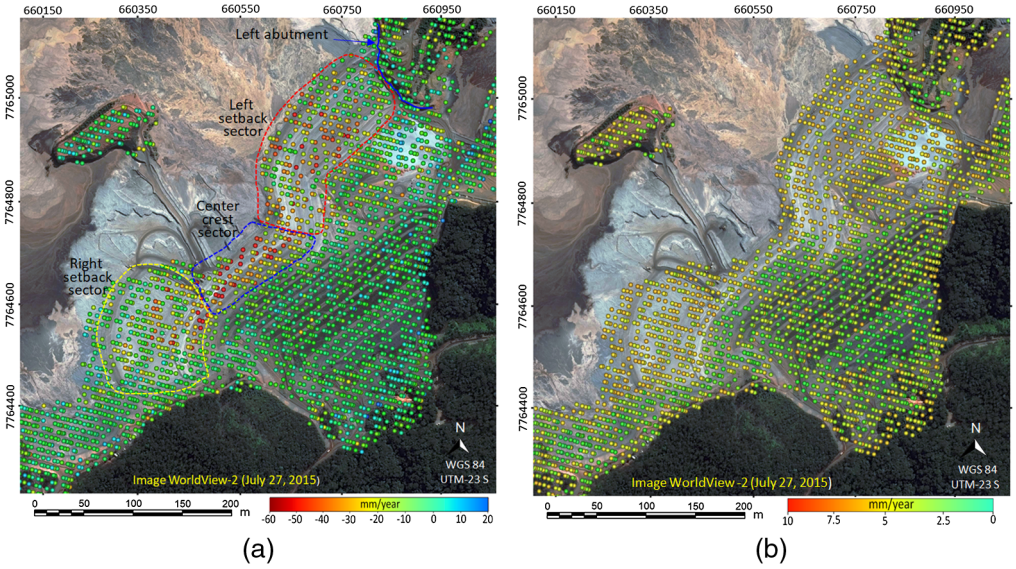

Fig. 5 (a) Ground displacement map in LOS at the Fundão dam from 14 S1A images and (b) the corresponding standard deviation map.

rate reached values from 20 to −60 mm/year and features LOS uplift and subsidence in the dam area. The standard deviation of the displacement rates depends on the distance from the reference point, which in this case was about 1200 m from the dam center; it also depends on the linearity and non-linearity deformation behavior [Fig. 5(b)]. Figure 6 shows a 3D representation of the Fundão dam and its corresponding reservoir.

The technical final report of the disaster concluded that the collapse of the Fundão dam was due to liquefaction, i.e., when solid materials (sandy tailings) lose their mechanical resistance and present fluid behavior.[3] It happened in the left abutment sector of the Fundão dam due to the change in the original design (setback) that caused an increase in saturation that introduced the potential for liquefaction. As a result, the slimes existing beneath the embankment were subject to load of the material above them, which consequently initiated a mechanism of extrusion of the slimes and pulling apart of the sands as the height of the embankment increased. Figure 7 shows the left setback sector of the Fundão dam and the positions of the prisms for topographic monitoring.

Downloaded From: https://www.spiedigitallibrary.org/journals/Journal-of-Applied-Remote-Sensing on 31 Aug 2021
Terms of Use: https://www.spiedigitallibrary.org/terms-of-use

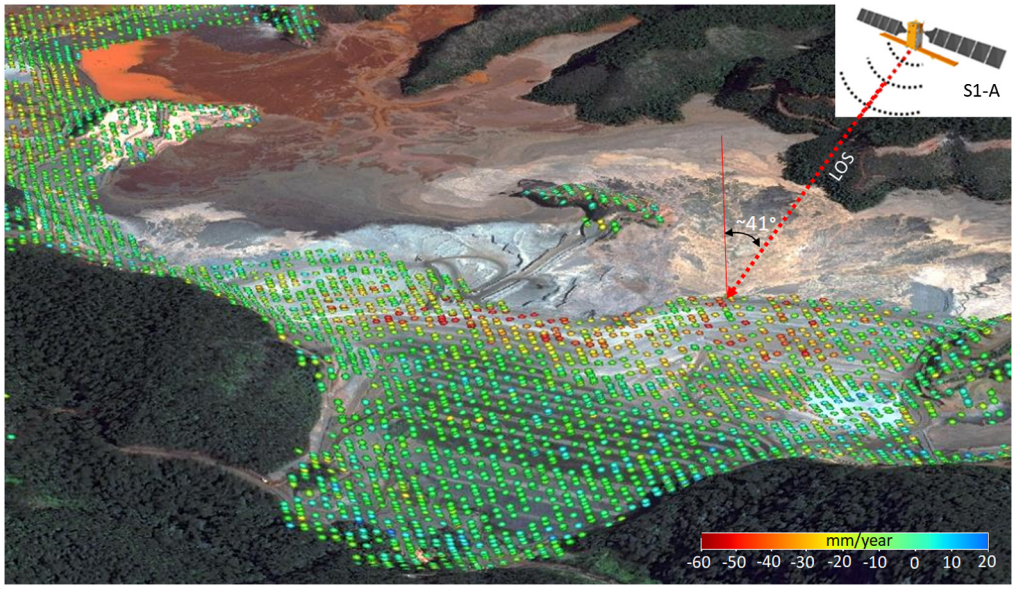

Fig. 6 Representation in 3D of the ground displacement of the Fundão dam and its corresponding reservoir.

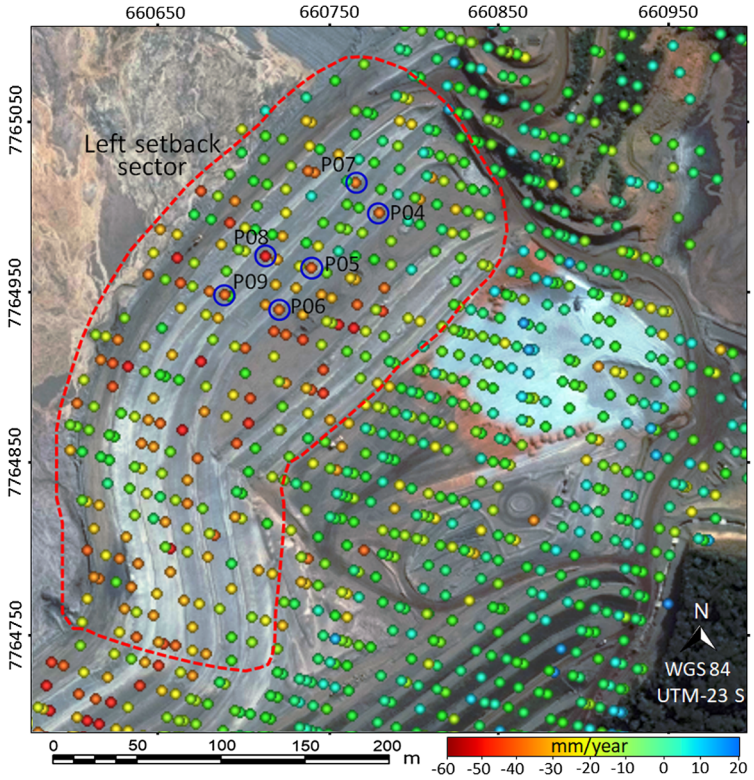

Fig. 7 Left setback sector of the Fundão dam and the positions of the six MPs analyzed close to the prisms positions.

The ground displacement graphs obtained by A-DInSAR of these six MPs are shown in Fig. 8. The time interval Δt_p in this figure, indicates the concomitant monitoring with the two techniques. The data from these six points monitored by total station/prisms were obtained from the technical report graphs from March 8, 2015, to August 18, 2015. The azimuth angles were estimated from the vector orientation of the horizontal displacement. Based on the orientation

Downloaded From: https://www.spiedigitallibrary.org/journals/Journal-of-Applied-Remote-Sensing on 31 Aug 2021
Terms of Use: https://www.spiedigitallibrary.org/terms-of-use

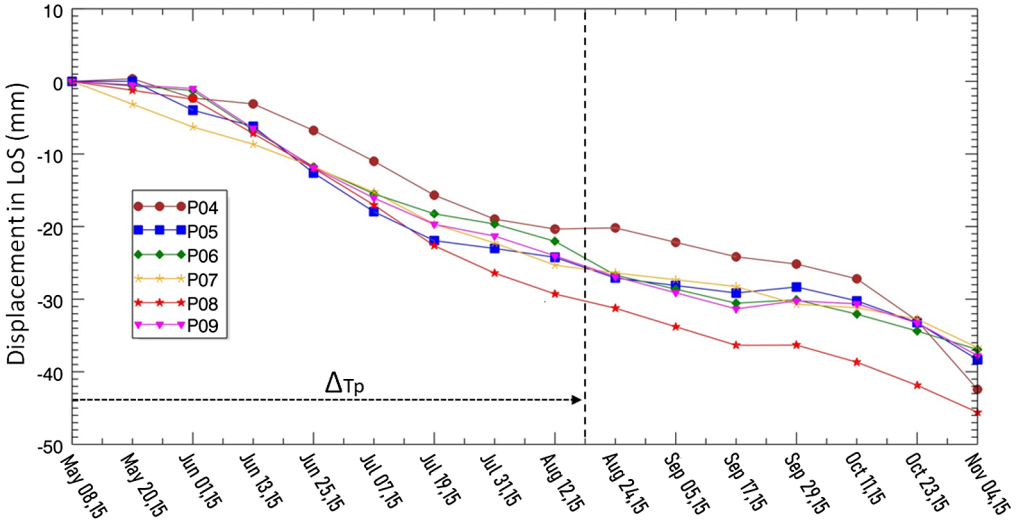

Fig. 8 PSI ground displacement in LOS for the six MPs analyzed.

angle ($\Theta az\_\Delta h$) and the horizontal (Δh) and vertical (Δv) displacement, it was possible to estimate the topographic displacement in the LOS direction. Table 3 shows the displacements in LOS for the six points for both types of measurements, topographic and PSI, during the time period Δt_p, as well as the approximated distances between the prism positions and the MPs. The discrepancy between the measurements could be related to its different positions (Δdist) and associated errors of the two techniques.

The PSI processing results performed after the accident in the Germano mining complex, from November 16, 2015, to May 15, 2017, are shown in Fig. 9. The critical structures analyzed in this work post-accident were the Sela&Tulipa dike, Selinha dike, and main Germano dam; in these structures, patterns of stability can be noticed. In the auxiliary dikes used for the access of trucks and heavy equipment and in the Baia 3 reservoir, patterns of the ground displacement can be observed.

During the period of Sentinel-1 acquisitions post-accident, sectors of the Germano mining complex were monitored with a total robotic station in several intermittent time intervals. The accumulated displacements measured in these intervals with the robotic station were compared with accumulated PSI results; the longest topographic interval was from August 9, 2016, to May 15, 2017. Topographic monitoring was accomplished with a Leica TM50 0.5 "(half second) robotic station, with 0.6 mm + 1 ppm nominal accuracy and Leica GPR112 prisms. With a longest monitoring distance of 815 m, the angular errors of the prisms and the station were 2.5" (two

Table 3 Accumulated displacement in LOS during the time period Δt_p for the topographic and PSI measurements.

Point ID	Topographic measurement parameters				PSI result	Distance (topo-PSI)
	Δv (mm)	Δh (mm)	$\Theta az\_\Delta h$ (deg)	Dtopo_LOS (mm)	Dpsi_LOS (mm)	Δdist (module) (m)
P04	−12	22	196	−24	−21	12
P05	−24	20	220	−28	−27	8
P06	−25	22	190	−32	−28	19
P07	−30	30	223	−36	−27	12
P08	−32	20	196	−36	−33	8
P09	−31	−10	162	−31	−28	20

Downloaded From: https://www.spiedigitallibrary.org/journals/Journal-of-Applied-Remote-Sensing on 31 Aug 2021
Terms of Use: https://www.spiedigitallibrary.org/terms-of-use

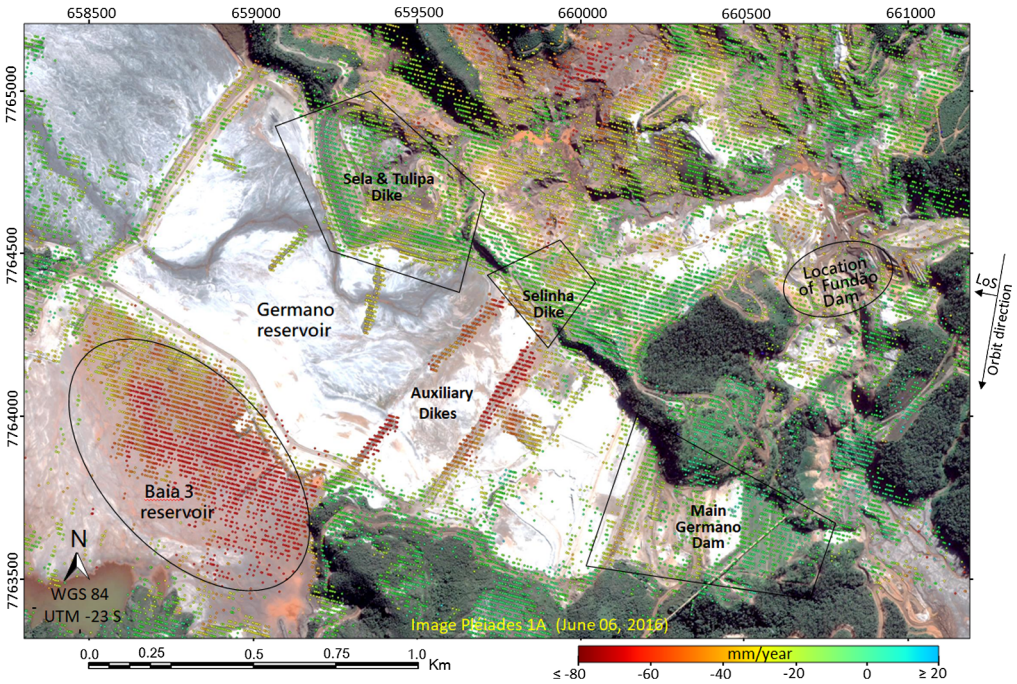

Fig. 9 Ground displacement map in LOS of the Germano mining complex.

and a half seconds), leading to a monitoring error (ME) of ±10 mm. As the zero reading can present the same nominal error in theory, the limit of two times the nominal error (accumulated error totalizing 20 mm) was established as a safety limit for the detection of movements according to the geotechnical team of the SAMARCO Company; this limit was used for the analysis of the results. In this way, values of vertical displacement projected in LOS (41 deg of incidence angle) within the interval of ±15 mm (bar error limits) were interpreted as accepted errors, while accumulated displacements outside this limit could indicate real deformations.

The PSI accuracy results depend mainly on the number of SAR images, spatial distribution of MP, weather conditions, precise DEM, distance from the reference point, and quality of MP within the area of interest. Typically, using datasets of more than 20 satellite images, errors on individual measurements are usually within ±5 mm.[19]

The structure that probably suffered the greatest impact of the accident was the Sela&Tulipa dike due to the immense volume of waste material that was abruptly removed from the other side of the dike. This dike was reinforced just before the accident, and the material placed on it was compacted during the period of the analysis. Figure 10 shows the Sela&Tulipa dike with details of the field pictures of the wall Fig. 10(a) and the ground displacement map of the dike and surrounding area with 18 points of in situ topographic measurements.

A comparison analysis was performed between the types of techniques, where the displacements measured by the total station on the prisms were projected in LOS of the satellite. Figure 11 shows the box plot of the accumulated displacement and standard deviation for the 18 points monitored with the robotic station and the PSI results in the Sela&Tulipa dike, performed during the period of November 16, 2015, to May 15, 2017. All prisms presented accumulated displacement within the error limit (±15 mm). The PSI results also exhibited low accumulated displacements for the 18 MPs analyzed (close to the prisms positions), except for ZI206, ZI212, ZI223, and ZI225, which slightly exceeded the error limit.

The MPs in Fig. 11 present values with a little discrepancy between the two techniques, which were probably caused by the different time intervals used to compare the results, with topographic measurements shorter than PSI. Furthermore the position of the prisms does not match perfectly with the PSI MPs. Nevertheless, most of the values were within the criterion of the error limit (±15 mm). This amount of displacement value did not compromise the stability of this structure, according to the geotechnical team of the SAMARCO Company.

Downloaded From: https://www.spiedigitallibrary.org/journals/Journal-of-Applied-Remote-Sensing on 31 Aug 2021
Terms of Use: https://www.spiedigitallibrary.org/terms-of-use

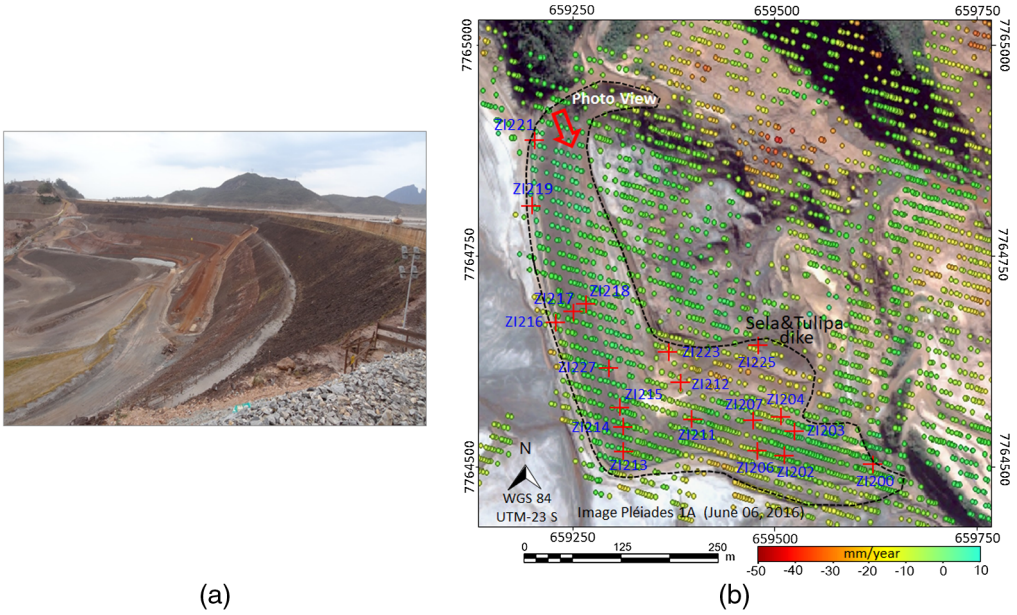

Fig. 10 (a) Picture of the wall of the Sela&Tulipa dike and (b) the displacement map showing the prisms positions and the dike location.

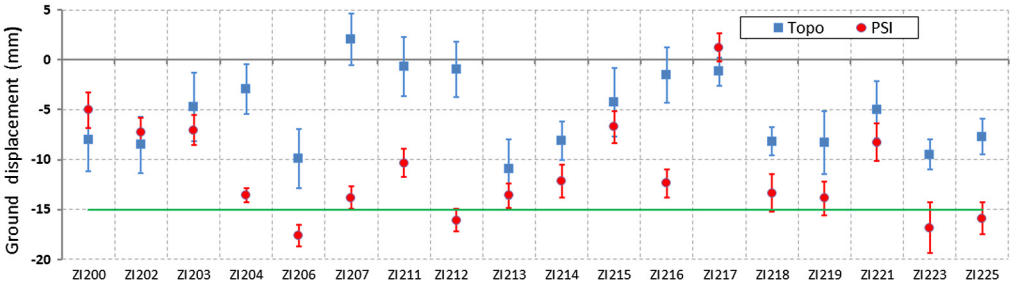

Fig. 11 Accumulated displacements from November 16, 2015, to May 15, 2017, for prisms (robotic station) and corresponding MP (close to the prisms positions) and its related standard deviations in the Sela&Tulipa dike. The error bar limit (−15 mm) is shown in green.

Another structure that made contact with the Fundão reservoir was the Selinha dike, shown in Fig. 12, with details of the field pictures of the wall [Fig. 12(a)] and the ground displacement map of the dike area showing 8 points of in situ topographic measurements [Fig. 12(b)].

The box plot of the accumulated displacement and standard deviation for the eight points monitored with the robotic station and PSI results in the Selinha dike is shown in Fig. 13, for the period of November 16, 2015, to May 15, 2017 All prisms presented accumulated displacement within the error limit (±15 mm). The PSI results exhibited accumulated displacements for the 8 MPs analyzed (close to the prisms positions), showing values within the error limits, except for ZI305, ZI307 and ZI308, which slightly exceeded the error limit. The cause of the discrepancy between the two measurements probably was the same as explained for the Sela&Tulipa dike.

The region of the Germano main dam did not suffer a direct impact of the rupture of the Fundão dam; only the buttress sector suffered minor damage and was corrected right after the accident. This dam can be divided in three sectors as shown in Fig. 14 in the field picture: (a) the upper sector, (b) the steepest sector, and (c) the buttress of the dam. Figure 15 shows the ground displacement map in these three sectors of the dam shown in Fig. 14. Patterns of stability can be seen in these three sectors, with (a) showing a small displacement rate due to its composition (waste material and sand) and the traffic on the tracks.

The PSI results were compared with in situ topographic measurement with the robotic station and prisms as shown in Fig. 16, which gives the box plot of the accumulated displacement

Downloaded From: https://www.spiedigitallibrary.org/journals/Journal-of-Applied-Remote-Sensing on 31 Aug 2021
Terms of Use: https://www.spiedigitallibrary.org/terms-of-use

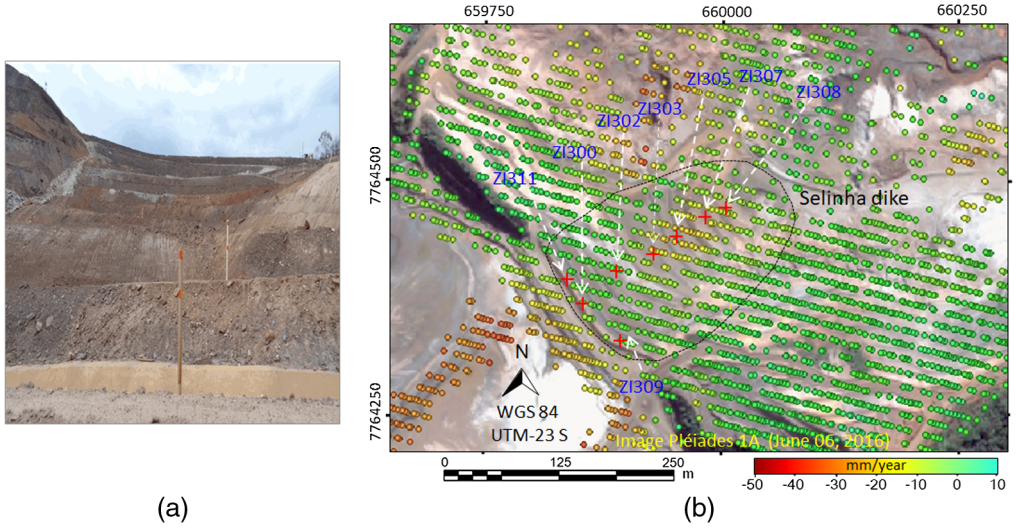

Fig. 12 (a) Picture of the wall of the Selinha dike and (b) the PSI displacement map showing the positions of the prisms and the dike location.

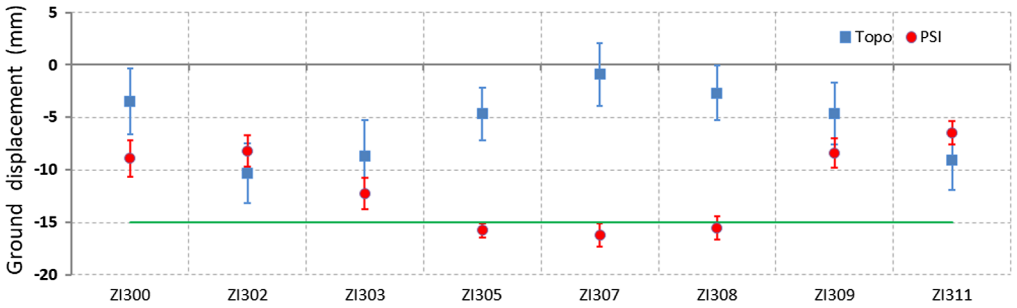

Fig. 13 Accumulated displacement from November 16, 2015, to May 15, 2017, for prisms and corresponding MPs (closest to the prisms positions) and its related standard deviations in the Selinha dike. The error bar limit (−15 mm) is shown in green.

Fig. 14 (a) Field pictures presenting the upper sector, (b) steepest sector, and (c) buttress sector of the main Germano dam.

(projected in LOS) and standard deviation for the 34 prisms monitored and the PSI results for the MPs close to the prisms positions, during the period of November 16, 2015, to May 15, 2017, in the main Germano dam. All prisms presented accumulated displacements within the error limit (±15 mm). PSI results also presented low accumulated displacements for the 34 MPs analyzed, showing most of the values within error bar limits.

Downloaded From: https://www.spiedigitallibrary.org/journals/Journal-of-Applied-Remote-Sensing on 31 Aug 2021
Terms of Use: https://www.spiedigitallibrary.org/terms-of-use

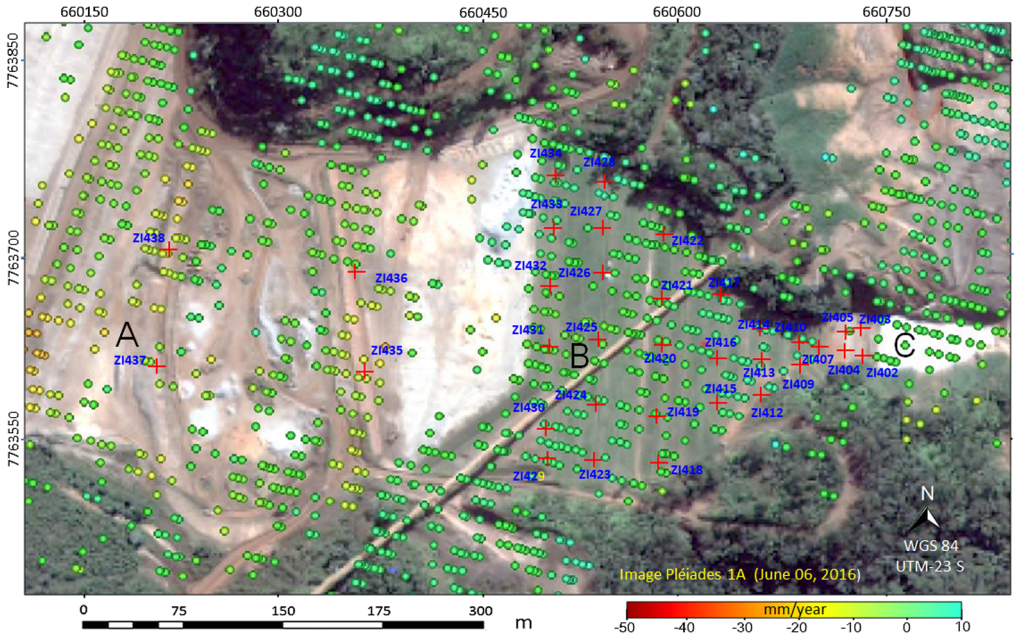

Fig. 15 PSI ground displacement map in LOS showing the positions of the prisms and (a) the upper sector, (b) steepest sector, and (c) buttress sector in the main Germano dam.

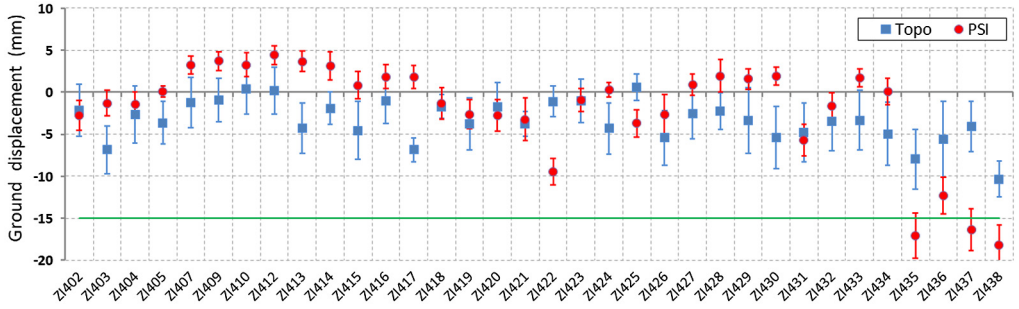

Fig. 16 Accumulated displacements from November 11, 2015, to May 15, 2017, for 34 prisms and corresponding MPs (closest to the prisms positions) and its related standard deviations in the main Germano dam. The error bar limit (−15 mm) is shown in green.

The presented results in Fig. 16 indicate stability in the main Germano dam, during the analysis interval, according to the safety criterion used by the geotechnical team of the SAMARCO Company. The MPs closer to the prisms ZI435, ZI437, and ZI438, located in the upper sector of the dam, show accumulated displacement slightly outside the error limit, as shown in Fig. 16. This sector of the Germano dam was built with a compact mixture of sand and silt-sized particles [Fig. 14(a)], which caused ground settlement due to the traffic of heavy vehicles and no deposition of material during the period of the PSI analysis. Furthermore, the disagreements between topographic and PSI measurements were caused probably by the different monitoring time intervals used to compare the results, with topographic measurement shorter than PSI, and considering that the position of the prisms did not matched perfectly with the PSI MPs.

Statistical tests were performed to verify if the PSI results would provide a similar ground displacement inference to the in situ geodetic measurement. The Wilcoxon test for paired data were carried out with the Sela&Tulipa dike results (Fig. 11), Selinha dike results (Fig. 13), and main Germano dam results (Fig. 16). This non-parametric statistical test was chosen considering the small number of samples and lack of knowledge of the data distribution. According to the Wilcoxon test results (Table 4), the measurements at the Selinha Dike and the main Germano dam show that the null hypothesis was not accepted, concluding that the PSI and the geodetic

Downloaded From: https://www.spiedigitallibrary.org/journals/Journal-of-Applied-Remote-Sensing on 31 Aug 2021
Terms of Use: https://www.spiedigitallibrary.org/terms-of-use

Table 4 Wilcoxon statistic test result at a significance level: $p < 0.05$ for PSI and geodetic data.

Location	Standard deviation of the geodetic accumulated displacement (mm)	Standard deviation of the PSI accumulated displacement (mm)	Wilcoxon test			
			N (cases)	T (W test)	*p*-value	$\mu_1 = \mu_2$
Sela&Tulipa dike	3.84	4.8	18	11	0.0012	ok
Selinhadike	2.47	2.63	8	5.0	0.0687	ok
Main Germano Dam	1.62	5.98	34	222	0.197	ok
Main Germano Dam[a]	1.32	3.11	31	92	0.004	ok

Significance level: p; number of cases: N; Wilcoxon test: T; median of a group of data: μ.
[a]Without prisms ZI435, ZI436, ZI437 and ZI438.

Fig. 17 Field picture of the auxiliary dike and the reservoir in the Germano mining complex.

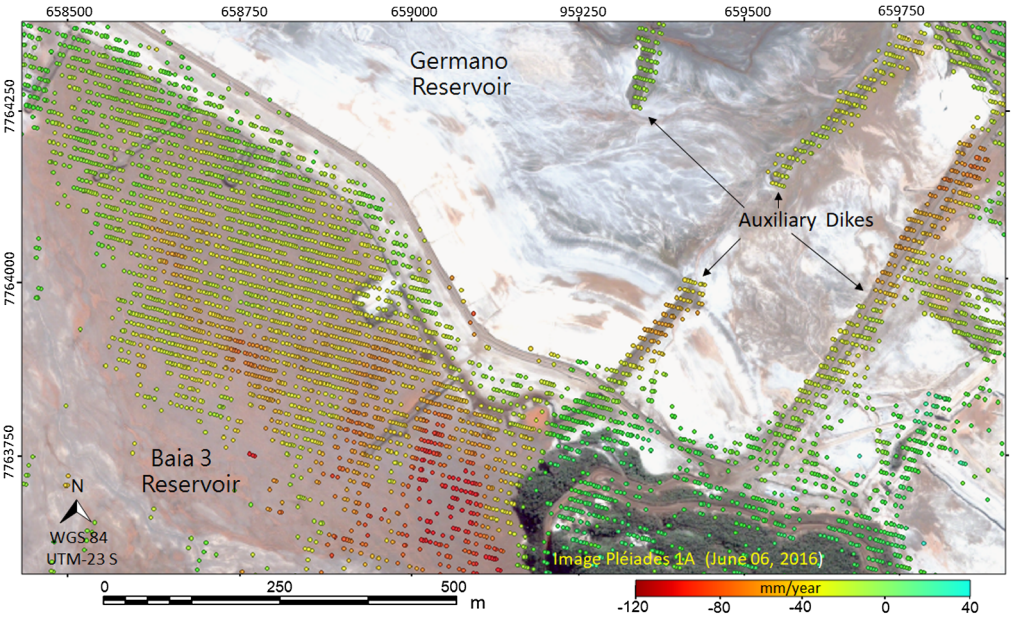

Fig. 18 PSI ground displacement map in LOS showing the auxiliary dikes and the Baia 3 reservoir.

Downloaded From: https://www.spiedigitallibrary.org/journals/Journal-of-Applied-Remote-Sensing on 31 Aug 2021
Terms of Use: https://www.spiedigitallibrary.org/terms-of-use

measurements have no similarity for a significance level of 5%; thus, the alternative hypothesis was accepted. For Sela&Tulipa and the main Germano dam* (without the prisms ZI435, ZI436, ZI437, and ZI438 with disparate values), the null hypothesis was accepted; therefore they showed similarity with significance level of <5%.

Others structures were analyzed in the Germano mining complex; a field picture of the sector containing auxiliary dikes and the reservoir in is shown in Fig. 17. Dikes are supporting structures that serve to delimit the areas for tailings impoundment, allowing for proper handling of material as well as access routes.

Figure 18 shows a ground displacement map containing the auxiliary dikes and the Baia 3 reservoir. These structures were the most affected in terms of ground deformation; since no deposition of material occurred after Fundão dam rupture, the soils in the reservoir underwent an overall compaction (settlement), reaching values of up to −120 mm/year. Furthermore, compaction also occurred on the auxiliary dikes caused by continuous traffic of heavy vehicles, reaching values of up to −90 mm/year.

7 Conclusions

With the integration of SBAS and PSI techniques, our propose methodology was able to detect deformation in the Fundão Dam prior to the disaster. The displacement rate reached values from 20 to −60 mm/year, featuring uplift and subsidence, detected during the monitoring period from May 8, 2015, to November 4, 2015, using Sentinel-1 images. In the left abutment sector of the Fundão dam, where the rupture started, six points (prisms) monitored with the robotic station were compared with PSI results and showed good agreement, despite the short time of simultaneous monitoring.

The analysis carried out after the disaster aimed to verify whether the results obtained with the A-DInSAR technique, using images from Sentinel-1 data, were similar to the results obtained with a topographic survey. The structures analyzed were the Sela&Tulipa dike, Selinha dike and main Germano dam. In general, the comparison between the two measurements techniques was quite similar, within the error limit established by the SAMARCO Company. A few points monitored by A-DInSAR slightly exceeded the error limit in the Sela&Tulipa dike and Selinha dike. In the main Germano dam, three points (ZI435, ZI437, and ZI438 prisms) crossed the limit a little more. Wilcoxon statistic tests were performed on the paired data of the Sela&Tulipa dike and main Germano dam results and both showed a good similarity (when ZI435, ZI436, ZI437, and ZI438 prisms were removed from the test). Based on the comparison between the two monitoring techniques, the conclusion is that the differences found among them were not significant, with both indicative of stability on the analyzed structures.

The deformation on the auxiliary dikes and in the Baia 3 reservoir reached values of −80 mm/year and −120 mm/year, respectively; these were caused by soil settlements and terrain compaction due to the continuous traffic of trucks.

Tailings dams are usually difficult to monitor due to their sizes, shapes, and inaccessibility sectors. However, to keep functioning while being considered structurally stable, constant monitoring and deformation assessment is needed, but it can be time-consuming and economically expensive. The stability of these structures is measured basically with in-situ geotechnical instruments as well as in visual inspections. With conventional systems, it is not always possible to cover a wide area; in addition, the displacements information is limited to a discrete number of survey points with robotic stations or sectors with ground-based radar.

A-DInSAR analysis is a reliable and powerful way to monitor stability evolution in time with a millimeter scale. When compared with conventional methods, its advantages are significant; it is possible to monitor a vast area with a high density of points without the need for any field visit or installation of equipment and provide a synoptic visualization of the displacement phenomenon over large areas in all-weather condition. This technique represents an economical way to monitor mining structures, saving costs and monitoring time, and can be used as a complementary analysis to detect movements in the tailings dams and their surrounding areas. Since this technique is not real-time monitoring, integration with topographic survey and ground-based radar is recommended for operational purposes

Downloaded From: https://www.spiedigitallibrary.org/journals/Journal-of-Applied-Remote-Sensing on 31 Aug 2021
Terms of Use: https://www.spiedigitallibrary.org/terms-of-use

This research demonstrated how A-DInSAR analysis, using Sentinel-1 SAR data, can be useful in detecting possible instability signals to avoid accidents and over large areas impacted by dam rupture, aiming at risk mitigation strategies.

Acknowledgments

The authors are grateful for the support of Visiona Tecnologia Epacial S.A., Airbus Defence & space, and Maxar Intelligence Inc. for providing the Pleiades 1A tri stereo and WorldView-2 stereo images for this research. The Conselho Nacional de Desenvolvimento Científico e Tecnológico (CNPq) is also acknowledged for a grant (CNPq Process: 304091/2019-7) received by the third author during the investigation. Finally, the authors are particularly grateful to the SAMARCO Company team in Mariana-MG for the support during the field work campaign and the topographic data. The article was significantly improved by the journal's reviewers.

References

1. C. A. Rosiere and V. K. Rolim, "Formações ferríferas e minério de alto teor associado: o minério de ferro no Brasil, geologia, metalogênese e economia," in *Recursos Minerais no Brasil, problemas e desafios*, pp. 2–45, Academia Brasileira de Ciências, Rio de Janeiro (2016).
2. F. F. Carmo et al., "Fundão tailings dam failures: the environment tragedy of the largest technological dissaster of Brazilian mining in global context," *Perspect. Ecol. Conserv.* **15**, 145–151 (2017).
3. N. R. Morgenstern et al., "Fundão Tailings Dam Review Panel: Report on the Immediate Causes of the Failure of the Fundão Dam," 2016, Samarco S.A., Vale S.A., BHP Brasil Ltd., p. 76, http://fundaoinvestigation.com/the-panel-report/ (accessed February 1, 2021).
4. H. Agurto-Detzel et al., "The tailings dam failure of 5 November 2015 in SE Brazil and its preceding seismic sequence," *Geophys. Res. Lett.* **43**, 8 (2016).
5. P. Berardino et al., "A new algorithm for surface deformation monitoring based on small baseline differential SAR interferogramas," *IEEE Trans. Geosci. Remote Sens.* **40**(11), 2375–2383 (2002).
6. A. Ferretti, C. Prati, and F. Rocca, "Permanent scatterers in SAR interferometry," *IEEE Trans. Geosci. Remote Sens.* **39**(1), 8–20 (2001).
7. C. Werner et al., "Interferometric point target analysis for deformation mapping," *IEEE Int. Geosci. Remote Sens. Symp., Proc. (IEEE Cat. No. 03CH37477)*, Toulouse (France), Vol. 7, pp. 4362–4364 (2003).
8. A. Hooper et al., "A new method for measuring deformation on volcanoes and other natural terrains using InSAR Persistent Scatterers," *Geophys. Res. Lett.* **31**, L23611 (2004).
9. C. Colesanti et al., "Detection of mining related ground instabilities using the permanent scatterers technique: a case study in the east of France," *Int. J. Remote Sens.* **26**(1), 201–207 (2005).
10. G. Herrera et al., "Mapping ground movements in open pit mining areas using differential SAR interferometry," *Int. J. Rock Mech. Mining Sci.* **47**, 1114–1125 (2010).
11. Z. Perski et al., "InSAR analyses of terrain deformation near the Wieliczka Salt Mine, Poland," *Eng. Geol.* **106**, 58–67 (2009).
12. Y. Guéguen et al., "Monitoring residual mining subsidence of Nord/Pas-de-Calais coal basin from differential and Persistent Scatterer Interferometry (Northern France)," *J. Appl. Geophys.* **69**, 24–34 (2009).
13. A.-H. Ng et al., "Mapping accumulated mine subsidence using small stack of SAR differential interferograms in the southern coalfield of New South Wales, Australia," *Eng. Geol.* **115**, 1–15 (2010).
14. U. Wegmüller et al., "Nonuniform ground deformation monitoring with TerraSAR-X persistent scatterer interferometry," *IEEE Trans. Geosci. Remote Sens.* **48**(2), 895–904 (2010).

Downloaded From: https://www.spiedigitallibrary.org/journals/Journal-of-Applied-Remote-Sensing on 31 Aug 2021
Terms of Use: https://www.spiedigitallibrary.org/terms-of-use

15. Z. Zhang et al., "Subsidence monitoring in coal area using time-series InSAR combining persistent scatterers and distributed scatterers," *Int. J. Appl. Earth Obs. Geoinf.* **39**, 49–55 (2015).
16. Z. Du et al., "Investigation on mining subsidence over Appin–West Cliff Colliery using time-series SAR interferometry," *Int. J. Remote Sens.* **39**(5), 1528–1547 (2017).
17. K. Pawluszek-Filipiak and A. Borkowski, "Monitoring mining induced subsidence by integrating differential radar interferometry and persistent scatterer techniques," *Eur. J. Remote Sens.* **54**, 1–13 (2021).
18. M. E. Hartwig, W. R. Paradella, and J. C. Mura, "Detection and monitoring of surface motions in active mine in the Amazon region, using persistent scatterer interferometry with TerraSAR-X satellite Data," *Remote Sens.* **5**, 4719–4734 (2013).
19. W. R. Paradella et al., "Mapping surface deformation in open pit iron mines of Carajás Province (Amazon Region) using an integrated SAR analysis," *Eng. Geol.* **193**, 61–78 (2015).
20. M. Przyłucka et al., "Combination of conventional and advanced A-DInSAR to monitor very fast mining subsidence with TerraSAR-X data: Bytom City (Poland)," *Remote Sens.* **7**, 5300–5328 (2015).
21. C. A. Pinto et al., "Applying persistent scatterer interferometry for surface displacement mapping in the Azul open pit manganese mine (Amazon region) with TerraSAR-X data," *J. Appl. Remote Sens.* **9**, 095978 (2015).
22. J. C. Mura et al., "Monitoring of non linear ground movement in an open pit iron mine based on an integration of advanced DInSAR techniques using TerraSAR-X data," *Remote Sens.* **8**, 409–427 (2016).
23. F. F. Gama et al., "Monitoring subsidence of open pit iron mines at Carajás Province based on SBAS interferometric technique using TerraSAR-X data," *Remote Sens. Appl. Soc. Environ.* **8**, 199–211 (2017).
24. G. G. Silva et al., "Monitoring of ground movement in open pit iron mines of Carajás Province (Amazon region) based on A-DInSAR techniques using TerraSAR-X data," *J. Appl. Remote Sens.* **11**, 026027 (2017).
25. J. C. Mura et al., "Monitoring the vulnerability of the dam and dykes in Germano iron mining after the collapse of the tailings dam of Fundão (Mariana-MG, Brazil using DInSAR techniques with TerraSAR-X data," *Remote Sens.* **10**, 1507 (2018).
26. W. Tang, M. Motagh, and W. Zhand, "Monitoring active open-pit mine stability in the Rhenish coalfields of Germany using a coherence-based SBAS method," *Int. J. Appl. Earth Obs. Geoinf.* **93**, 102217 (2020).
27. F. G. Gama et al., "Deformations prior to the Brumadinho dam collapse revealed by Sentinel-1 InSAR data using SBAS and PSI techniques," *Remote Sens.* **12**, 3664 (2020).
28. R. Osmanoglu et al., "Time series analysis of InSAR data: methods and trends," *ISPRS J. Photogramm. Remote Sens.* **115**, 90–102 (2016).
29. M. Constantini, "A novel phase-unwrapping algorithm based on network programming," *IEEE Trans. Geosci. Remote Sens.* **36**(3), 813–820 (1998).
30. G. Golub and C. Loan, *Matrix Computations*, 3rd ed., pp. 427–435, John Hopkins University Press, Baltimore (1996).
31. "GAMMA remote sensing," https://www.gamma-rs.ch (accessed Dec. 01, 2020).

José C. Mura received his BS degree in electrical engineering from the University of São Paulo (USP-EESC), Brazil, in 1978, his MS degree in electronics and telecommunications from the Aeronautics Institute of Technology (ITA), Brazil, in 1985, and his PhD in applied computer science from INPE in 2000. He has been at the INPE since 1979 (In 1992–1993, he was with DLR, Germany, as a guest scientist). His main research interests include radar remote sensing applications and SAR interferometric processing.

Fábio F. Gama is an electronic engineer and received his PhD in 2007 in radar remote sensing. He currently works at the National Institute for Space Research (INPE-Brazil) as a senior researcher at the Earth Observation and Geoinformatics Division, with SAR applications, particularly in estimation of surface deformation using advanced differential interferometric techniques.

Downloaded From: https://www.spiedigitallibrary.org/journals/Journal-of-Applied-Remote-Sensing on 31 Aug 2021
Terms of Use: https://www.spiedigitallibrary.org/terms-of-use

Waldir R. Paradella is a geologist with a BS in geology from the University of São Paulo (USP), Brazil, in 1973, an MS in remote sensing from INPE in 1976, and a PhD in geology from USP in 1983. Since 1974, he has been with INPE and currently is a senior researcher. (In 1988 and 1995, he was with CCRS, Canada, as a postdoctoral fellow and visiting scientist.) His main research interests include geoscience applications in tropical environments with SAR.

Cleber G. de Oliveira holds a degree in cartographic engineering from the Universidade Estadual Paulista – UNESP (1997) and holds the titles of master (2005) and doctor (2011) in remote sensing from the National Institute for Space Research (INPE). He has worked in the geosciences area since 1998, and since 2015 he has worked at Visiona Tecnologia Espacial S.A. company, a Brazilian Space System Integration company.

Thiago G. Rodrigues: is graduated in cartographic engineering in Universidade Estadual Paulista UNESP in 2007 and MSc degree in remote sensing in National Institute for Space Research (INPE) in 2010, MBA in project management in Getulio Vargas Foundation (FGV) in 2015 and Project Management Professional (PMP) for Project Management Institute (PMI) in 2015 and since 2015 has worked at Visiona Tecnologia Espacial S.A. company, a Brazilian Space System Integration company.

Downloaded From: https://www.spiedigitallibrary.org/journals/Journal-of-Applied-Remote-Sensing on 31 Aug 2021
Terms of Use: https://www.spiedigitallibrary.org/terms-of-use